A recursive multibody model of a tracked vehicle and its interaction with flexible ground

Ray P.S. Han†

Department of Mechanical Engineering, The University of Iowa, Iowa City, IA 52242, USA

Brian S. Sander‡

Henderson Engineers Incorporated, Lenexa, KS 66214, USA

S.G. Mao‡†

Department of Mechanical Engineering, The University of Iowa, Iowa City, IA 52242, USA

Abstract. A high-fidelity model of a tracked vehicle traversing a flexible ground terrain with a varying profile is presented here. In this work, we employed a recursive formulation to model the track subsystem. This method yields a minimal set of coordinates and hence, computationally more efficient than conventional approaches. Also, in the vehicle subsystem, the undercarriage frame is assumed to be connected to the chassis by a revolute joint and a spring-damper unit. This increase in system mobility makes the model more realistic. To capture the vehicle-ground interaction, a Winkler-type foundation with springs-dampers is used. Simulation runs of the integrated tracked vehicle system for vibrations for four varying ground profiles are provided.

Key words: tracked vehicles; multibody dynamic models; flexible ground terrain; varying ground profile.

1. Introduction

Tracked vehicles can be broadly classified as high and low speed vehicles. High-speed tracked vehicles generally have a suspension for each roller of the undercarriage. A tank is a typical example of such a vehicle. Track models of high-speed vehicles are generally approximated without considering the individual track links. This is because the ride characteristics of these vehicles are more affected by the constraining effects of the track than the vibrations of the track loop. Some noted works in the modeling of high-speed tracked vehicles include McCullough and Haug (1985) who modeled the effects of the track using a superelement representation for the track with catenary equations, contact forces, and other track loop influences to account for a varying track tension. Galaitsis (1984) presented a dynamic simulation model for a tank that incorporated individual track

---

† Professor
‡ Engineer
‡† Graduate Student

links, so that the effects of slow speed motion can be captured. Dhir and Sankar (1994) proposed two track models and compared them with that of McCullough and Haug, and the track model in the VEHDYN code developed by Murphy and Ahlvin (1976), and Creighton (1986). These four analytical track models for high-speed vehicles were compared to experimental data. The two proposed track models and that of McCullough and Haug produced results very similar to the experimental measurements, while the VEHDYN code did not compare well with the measured data.

Low-speed tracked vehicles generally do not have a suspension for each individual roller. Examples of these vehicles include excavators and crawlers. To accurately capture the vibrational behavior of the vehicle, it is necessary to model the individual links for this type of vehicle. Nakanishi and Shabana (1994a) created a multibody model of an excavator in which the vehicle chassis and the track interact with each other through contact forces that are calculated based on stiffness and damping coefficients. Each track link and shoe are modeled as a separate body. Nakanishi and Shabana (1994b) compared their tracked vehicle model obtained through a global Cartesian formulation to one created with the recursive equations of motion. They concluded that the recursive method is computationally faster than the global Cartesian approach. Further efficiencies can be realized by recasting the model as a Hamiltonian system and then, carry out the numerical integration via symplectic algorithms (Han and Mao 1999).

2. Modeling the tracked vehicle

As illustrated in Fig. 1, a tracked vehicle such as a crawler can be modeled as consisting of two subsystems (Han, Mao and Sander 1999). The first is the track subsystem which consists of track links that are connected by revolute joints and held in place by the sprocket, idler, lower rollers and carrier roller. The second is the vehicle subsystem which comprises of the following bodies; cab, chassis, sprocket, idler, undercarriage frame, lower rollers and carrier roller. While there is dynamic force coupling between two subsystems, there is no inertia coupling since the kinematic equations of the subsystems are not coupled.
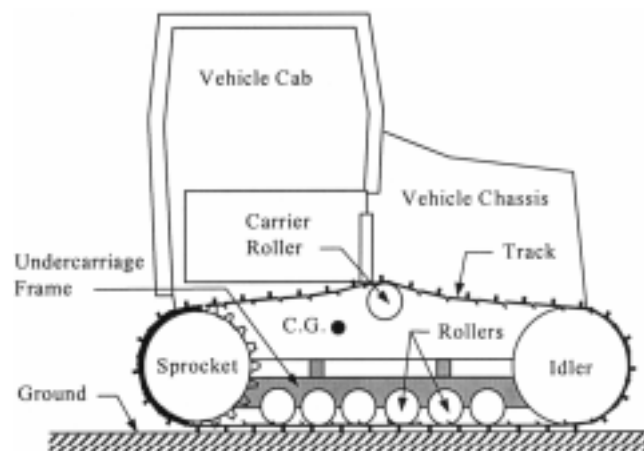

Fig. 1 Typical crawler components

3. Modeling the track subsystem

The track of an undercarriage in Fig. 1 is driven by a sprocket and guided by an idler, a series of rollers at the bottom, and a carrier roller at the top. This design is typically used for low speed vehicles. To better capture the effects of the vibration of the track and its interaction with the undercarriage components and the ground, individual track links are included in the model. The details of the various track components are highlighted in Fig. 2.

Each body of the track consists of mass and inertia values of the track link, track shoe with grouser, and one pin and bushing as sketched. The track is modeled as a closed loop of rigid track links connected by revolute joints. The equations of motion of the track are developed using a recursive formulation and being a closed loop system, the track must be cut to form 2 open loop chains connected to a base body as sketched in Fig. 3. Each body in the loop is defined with respect to its inboard body and a relative joint coordinate. Recursive kinematics are then employed to determine the Cartesian coordinates of all bodies, given the position of their inboard body and the relative joint coordinate. Full details of the recursive formulation are provided in the M.S. thesis of Sander (1998).

3.1 Recursive kinematics

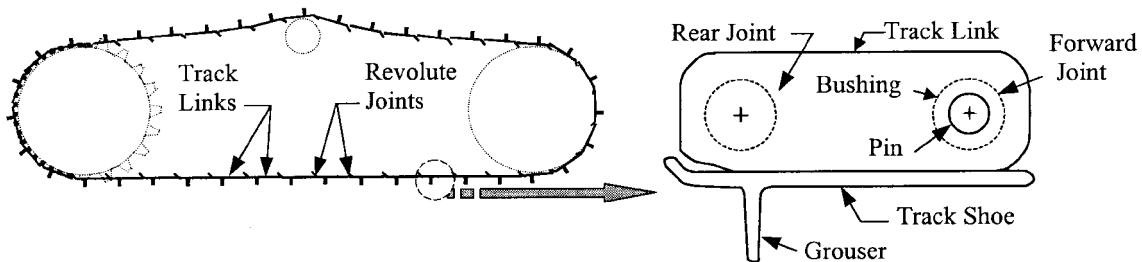Fig. 4 shows two planar bodies connected by a revolute joint. The relative joint coordinate is the

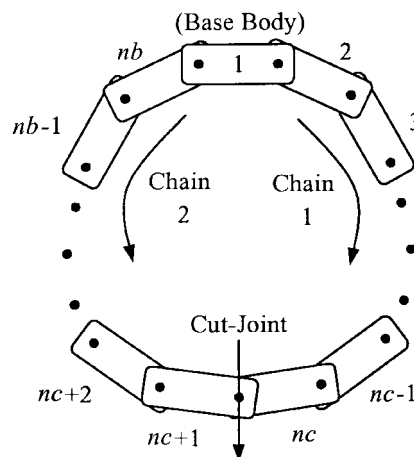Fig. 2 Model of the track subsystem
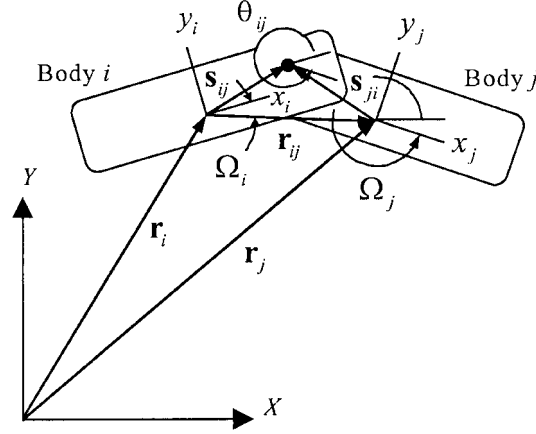

Fig. 3 Closed loop with cut-joint

Fig. 4 Two bodies connected by a revolute joint

rotation θ_{ij}. The global position vectors r_i and r_j locate body reference frame at the center of gravity of each body, and the vectors s_{ij} and s_{ji} located the joints with respect to the body reference frame. The recursive position relationship between an inboard body and an outboard body is

$$r_j = r_i + r_{ij} \tag{1}$$

where $r_{ij} = s_{ij} - s_{ji}$. Note that the joint vectors in the global frame, s_{ij} and s_{ji} are obtained by transforming the local, body-fixed joint vectors, s'_{ij} and s'_{ji} to the global reference frame using the transformation matrix $A(\Omega_i)$ which is a function of the orientation of the body with the joint vector fixed. The recursive velocity relationship is obtained by differentiating Eq. (1) with respect to time. The angular velocity of body j, $\dot{\Omega}_j$ is based on the angular velocity of body i and the relative angular velocity between bodies i and j. For the case of a planar revolute joint, the recursive kinematic equation for the outboard body angular position and angular velocity are the scalar equations

$$\Omega_j = \Omega_i + \theta_{ij} \tag{2}$$

and
$$\dot{\Omega}_j = \dot{\Omega}_i + \dot{\theta}_{ij} \tag{3}$$

The velocity of the joint vectors is due only to the rotation of the rigid body to which they belong. This velocity is found by taking the cross product of the angular velocity vector of the rigid body ω with the joint vector. That is,

$$\dot{s}_{ij} = \omega_i \times s_{ij} = \Omega_i \{-s_{ij,y} \quad s_{ij,x}\}^T, \tag{4}$$

in which $\omega_i = \Omega_i \hat{k}$; $\hat{k}$ unit vector in the positive z-axis and $s_{ij,y}, s_{ij,x}$ are the y and x-components of s_{ij}, respectively. The recursive velocity relationships between bodies i and j are collected into one set of equations given by,

$$Y_j \equiv \begin{Bmatrix} \dot{r}_j \\ \dot{\Omega}_j \end{Bmatrix} = \begin{bmatrix} 1 & 0 & -r_{ij,x} \\ 0 & 1 & r_{ij,x} \\ 0 & 0 & 1 \end{bmatrix} \begin{Bmatrix} \dot{r}_i \\ \dot{\Omega}_i \end{Bmatrix} + \begin{Bmatrix} s_{ji,y} \\ -s_{ji,x} \\ 1 \end{Bmatrix} \dot{\theta}_{ij} = B_{ij1} Y_i + B_{ij2} \dot{\theta}_{ij} \tag{5}$$
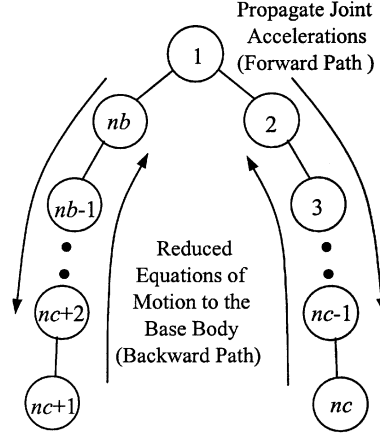
Fig. 5 Recursive calculation flow

Note that Y_j is the velocity vector of an outboard body j, given the velocity vector Y_i of its inboard body i. The recursive acceleration equation is obtained by time differentiating Eq. (5)

$$\dot{Y}_j = B_{ij1}\dot{Y}_i + B_{ij2}\ddot{\theta}_{ij} + D_{ij} \tag{6}$$

where the velocity coupling term $D_{ij} = \dot{B}_{ij1}Y_i + \dot{B}_{ij2}\dot{\theta}_{ij}$ contains the time derivatives of the coefficient matrices.

3.2 Recursive equations of motion

As shown in Fig. 5, two directions are employed in the recursive calculation flow: forward and backward path propagations. The equations of motion are further reduced to that for the base body and they include the constraint equations at the cut-joints. These equations are solved for the base body acceleration, as well as the Lagrange multipliers associated with the cut-joints. Recursive equations are then employed to forward propagate the relative joint accelerations. Defining the virtual displacements pertaining to the generalized coordinates of one body of the track by $\delta Z_j = \{\delta r_j \quad \delta \pi_j\}^T$, its recursive equation can be expressed as,

$$\delta Z_j = B_{ij1}\delta Z_i + B_{ij2}\delta \theta_{ij} \tag{7}$$

Applying the principle of virtual work to the closed loop system and for kinematically admissible virtual displacements δZ, we get the following variational equation of motion

$$\sum_{i=1}^{nb} \delta Z_i^T (M_i\dot{Y}_i - Q_i) + \sum_{i=nc}^{nc+1} \delta Z_i^T \Phi_{Z_i}^{(nc,\,nc+1)T}\lambda_{nc,\,nc+1} = 0 \tag{8}$$

The mass matrix M_i and the generalized force vector Q_i for each body are given as

$$M_i = \begin{bmatrix} m_i & 0 & 0 \\ 0 & m_i & 0 \\ 0 & 0 & I_{zz} \end{bmatrix} \text{ and } Q_i = \begin{bmatrix} f_i \\ n_i \end{bmatrix} \tag{9}$$

where the force vector f_i is in the global frame and n_i is the moment applied to the body about the

z-axis. The generalized force vector includes external forces applied to a body and that due to gravity. For closed loop systems, the Lagrange multiplier λ are related to the constraint forces at the cut-joint. For the revolute joint, the constraint equation is

$$\boldsymbol{\Phi}^{(nc,\,nc+1)} = \boldsymbol{r}_{nc} + \boldsymbol{A}_{nc}\boldsymbol{s}'_{nc,\,nc+1} - \boldsymbol{r}_{nc+1} - \boldsymbol{A}_{nc+1}\boldsymbol{s}'_{nc+1,\,nc} = \boldsymbol{0} \tag{10}$$

The constraint Jacobians of this equation for bodies *nc* and *nc*+1 are shown explicitly as

$$\boldsymbol{\Phi}^{(nc,\,nc+1)}_{Z_{nc}} = \begin{bmatrix} 1 & 0 & -\sin(\Omega_{nc})s'_{(nc,\,nc+1),\,x} - \cos(\Omega_{nc})s'_{(nc,\,nc+1),\,y} \\ 0 & 1 & \cos(\Omega_{nc})s'_{(nc,\,nc+1),\,x} - \sin(\Omega_{nc})s'_{(nc,\,nc+1),\,y} \end{bmatrix} \tag{11}$$

$$\boldsymbol{\Phi}^{(nc,\,nc+1)}_{Z_{nc+1}} = \begin{bmatrix} -1 & 0 & \sin(\Omega_{nc+1})s'_{(nc+1,\,nc),\,x} + \cos(\Omega_{nc+1})s'_{(nc+1,\,nc),\,y} \\ 0 & -1 & -\cos(\Omega_{nc+1})s'_{(nc+1,\,nc),\,x} + \sin(\Omega_{nc+1})s'_{(nc+1,\,nc),\,y} \end{bmatrix} \tag{12}$$

where the Jacobian is defined by

$$\boldsymbol{\Phi}^{(nc,\,nc+1)}_{Z_i} \equiv \left[\frac{\partial \boldsymbol{\Phi}^{(nc,\,nc+1)}}{\partial x_i} \frac{\partial \boldsymbol{\Phi}^{(nc,\,nc+1)}}{\partial y_i} \frac{\partial \boldsymbol{\Phi}^{(nc,\,nc+1)}}{\partial \Omega_i} \right] \tag{13}$$

Note that from this point onwards, the subscripts and superscripts $(nc,\,nc+1)$ denoting the cut-joint in Φ and λ terms are omitted for brevity. Substituting Eqs. (6) and (7) into Eq. (8), and noting that $\delta\theta$ is arbitrary, the variational equation of motion for the closed loop system of bodies connected by revolute joints is (Bae and Haug 1987):

$$\sum_{i=1}^{nc-2} \delta\boldsymbol{Z}_i^T(\boldsymbol{M}_i\dot{\boldsymbol{Y}}_i - \boldsymbol{Q}_i) + \delta\boldsymbol{Z}_{nc-1}^T\left\{ (\boldsymbol{M}_{nc-1} + \boldsymbol{K}_{nc-1})\dot{\boldsymbol{Y}}_{nc-1} - (\boldsymbol{Q}_{nc-1} + \boldsymbol{L}_{nc-1}) + \overline{\boldsymbol{M}}_{nc-1}^T\lambda \right\}$$

$$+ \sum_{i=nc+2}^{nb} \delta\boldsymbol{Z}_i^T(\boldsymbol{M}_i\dot{\boldsymbol{Y}}_i - \boldsymbol{Q}_i) + \delta\boldsymbol{Z}_{nc+1}^T\left(\boldsymbol{M}_{nc+1}\dot{\boldsymbol{Y}}_{nc+1} - \boldsymbol{Q}_{nc+1} + \boldsymbol{\Phi}_{Z_{nc+1}}^T\lambda \right) \tag{14}$$

In Eq. (14) the coefficients of $\dot{\boldsymbol{Y}}_{nc-1}$ are in $\boldsymbol{K}_{nc-1}$, while the coefficients of λ are in $\overline{\boldsymbol{M}}_{nc-1}^T$ and the remaining terms corresponding to forces and accelerations are grouped in $\boldsymbol{L}_{nc-1}$. These new terms are given by,

$$\boldsymbol{K}_{nc-1} = \boldsymbol{B}_{(nc-1)nc1}^T\boldsymbol{M}_{nc}\boldsymbol{B}_{(nc-1)nc1} - \boldsymbol{B}_{(nc-1)nc1}^T\boldsymbol{M}_{nc}\boldsymbol{B}_{(nc-1)nc2}$$
$$\times \left(\boldsymbol{B}_{(nc-1)nc2}^T\boldsymbol{M}_{nc}\boldsymbol{B}_{(nc-1)nc2} \right)^{-1}\left(\boldsymbol{B}_{(nc-1)nc2}^T\boldsymbol{M}_{nc}\boldsymbol{B}_{(nc-1)nc1} \right), \tag{15}$$

$$\boldsymbol{L}_{nc-1} = \boldsymbol{B}_{(nc-1)nc1}^T(\boldsymbol{Q}_{nc} - \boldsymbol{M}_{nc}\boldsymbol{D}_{(nc-1)nc}) + \boldsymbol{B}_{(nc-1)nc1}^T\boldsymbol{M}_{nc}\boldsymbol{B}_{(nc-1)nc2}$$
$$\times \left(\boldsymbol{B}_{(nc-1)nc2}^T\boldsymbol{M}_{nc}\boldsymbol{B}_{(nc-1)nc2} \right)^{-1}\boldsymbol{B}_{(nc-1)nc2}^T\left(\boldsymbol{M}_{nc}\boldsymbol{D}_{(nc-1)nc} - \boldsymbol{Q}_{nc} \right), \tag{16}$$

and $\overline{\boldsymbol{M}}_{nc-1}^T = \boldsymbol{B}_{(nc-1)nc1}^T\left\{ \boldsymbol{\Phi}_{Z_{nc}}^T - \boldsymbol{M}_{nc}\boldsymbol{B}_{(nc-1)nc2} \times \left(\boldsymbol{B}_{(nc-1)nc2}^T\boldsymbol{M}_{nc}\boldsymbol{B}_{(nc-1)nc2} \right)^{-1}\boldsymbol{B}_{(nc-1)nc2}^T\boldsymbol{\Phi}_{Z_{nc}}^T \right\}$ (17)

Since $\delta\theta$ must be arbitrary, its coefficient in Eq. (14) can be set to zero and this yields an expression for evaluating the relative joint acceleration

$$\ddot{\theta}_{j(j+1)} = -\left\{ \boldsymbol{B}_{j(j+1)2}^T(\boldsymbol{M}_{j+1} + \boldsymbol{K}_{j+1})\boldsymbol{B}_{j(j+1)2} \right\}^{-1}\left[\boldsymbol{B}_{j(j+1)2}^T(\boldsymbol{M}_{j+1} + \boldsymbol{K}_{j+1}) \times \boldsymbol{B}_{j(j+1)1}\dot{\boldsymbol{Y}}_j + \boldsymbol{B}_{j(j+1)2}^T \right.$$

$$\times \left\{ \left(M_{j+1} + K_{j+1} \right) D_{j(j+1)} - \left(Q_{j+1} + L_{j+1} \right) + \overline{M}_{j+1}^T \lambda \right\} \Big] \tag{18}$$

The final reduced variational equation of motion is obtained by mathematical induction from each cut-joint body to the base body along both chains of the closed loop. The result is (Sander 1998):

$$\delta Z_1^T \left\{ \left(M_1 + K_1^1 + K_1^2 \right) \dot{Y}_1 - \left(Q_1 + L_1^1 + L_1^2 \right) + \left(\overline{M}_1^{1T} + \overline{M}_1^{2T} \right) \lambda \right\} = \mathbf{0} \tag{19}$$

in which the superscripts on K_1, L_1, and $\overline{M}_1^T$ denote the chain from which the matrix was reduced. Eq. (19) cannot yet be solved for the generalized coordinate accelerations and Lagrange multipliers because there are 2 more unknowns than equations. For the track model with revolute joints, 2 additional constraint equations can be generated from the cut-joint acceleration equation to the bodies inboard of the cut-joint bodies:

$$\ddot{\Phi} = \overline{M}_{nc-1} \dot{Y}_{nc-1} + \overline{M}_{nc+2} \dot{Y}_{nc+2} + \left(\overline{L}_{nc-1} + \overline{L}_{nc+2} \right) \lambda - \mathbf{RHS}_{nc-1} - \mathbf{RHS}_{nc+2} - \gamma = \mathbf{0} \tag{20}$$

where

$$\overline{L}_{nc-1} = -\Phi_{Z_{nc}} B_{(nc-1)nc2} \left(B_{(nc-1)nc2}^T M_{nc} B_{(nc-1)nc2} \right)^{-1} B_{(nc-1)nc2}^T \Phi_{Z_{nc}}^T \tag{21}$$

$$\mathbf{RHS}_{nc-1} = \Phi_{Z_{nc}} \Big[B_{(nc-1)nc2} \left(B_{(nc-1)nc2}^T M_{nc} B_{(nc-1)nc2} \right)^{-1} B_{(nc-1)nc2}$$
$$\times \left(M_{nc} D_{(nc-1)nc} - Q_{nc} \right) - D_{(nc-1)nc} \Big] \tag{22}$$

The reduction of the constraint acceleration equations is continued from each of the cut-joints down their respective chain to the base body. By mathematical induction, the following cut-joint constraint acceleration equation at the base body is obtained:

$$\left(\overline{M}_1^1 + \overline{M}_1^2 \right) \dot{Y}_1 + \left(\overline{L}_1^1 + \overline{L}_1^2 \right) \lambda - \mathbf{RHS}_1^1 - \mathbf{RHS}_1^2 - \gamma = \mathbf{0} \tag{23}$$

Since the base body is not constrained by any external kinematic constraints, δZ_1 is thus arbitrary, allowing Eq. (19) to be simplified to

$$K_1 \dot{Y}_1 + \overline{M}_1^T \lambda = L_1 \tag{24}$$

and Eq. (23) to

$$\overline{M}_1 \dot{Y}_1 + \overline{L}_1 \lambda = \mathbf{RHS}_1 \tag{25}$$

where

$$K_1 = M_1 + K_1^1 + K_1^2 \; ; \; \overline{M}_1^T = \overline{M}_1^{1T} + \overline{M}_1^{2T} \; ; \; \overline{L}_1 = \overline{L}_1^1 + \overline{L}_1^2 \; ; \; \mathbf{RHS}_1 = \mathbf{RHS}_1^1 + \mathbf{RHS}_1^2 + \gamma \tag{26}$$

Appending the cut-joint constraint acceleration equations to the variational equations of motion yields a complete solvable set of equations for the motion of the system (see Han and Zhao 1990). In matrix form, we have:

$$\begin{bmatrix} K_1 & \overline{M}_1^T \\ \overline{M}_1 & \overline{L}_1 \end{bmatrix} \begin{bmatrix} \dot{Y}_1 \\ \lambda \end{bmatrix} = \begin{bmatrix} L_1 \\ \mathbf{RHS}_1 \end{bmatrix} \tag{27}$$

Eq. (27) can be solved for the base body acceleration and the Lagrange multipliers which are related to the constraint forces of the cut-joint. The results can then be substituted into Eq. (18) to solve for the relative joint acceleration between the base body and the first outboard body. The joint acceleration can be substituted into the recursive acceleration Eq. (6) to find the Cartesian acceleration of the first outboard body. This process is continued down each chain of the track until acceleration of the body preceding the cut-joint body has been calculated ($nc-1$ or $nc+2$). At this point the final relative joint accelerations $\ddot{\theta}_{(nc-1)nc}$ and $\ddot{\theta}_{(nc+2)(nc+1)}$ can be easily determined.

Table 1. Algorithm for solving the recursive equations of motion

Equation		Purpose and Comments
$q \begin{pmatrix} \Omega_1, \theta_{ij}, x_1, y_1 \\ \dot{\Omega}_1, \dot{\theta}_{ij}, \dot{x}_1, \dot{y}_1 \end{pmatrix}$		The process of calculating the system acceleration begins with knowledge of the initial positions and velocities of all track links. This information is contained in the vector q as Cartesian coordinates and velocities for the base body and relative joint coordinates and velocities for all other track links.
Ω_j r_j Y_j	Eq. (2) Eq. (1) Eq. (5)	This is the first step in calculating the equations of motion. The Cartesian position and velocity are calculated recursively along a forward path from the relative joint coordinates.
$Q_i(\Omega_i, r_i, Y_i)$ Eq. (9)		Externally applied forces are calculated as functions of the orientation, position, and velocity of the body. The model for calculating contact forces is discussed in Section 3.5
K_{nc-1} L_{nc-1} $\overline{M}_{nc-1}^T$ $\overline{L}_{nc-1}$ $\mathbf{RHS}_{nc-1}$	Eq. (15) Eq. (16) Eq. (17) Eq. (21) Eq. (22)	These matrix and vector terms are calculated recursively backwards from the chain-end bodies to the base body. When the base body is reached, the terms K_1, L_1, $\overline{M}_1^T$, $\overline{L}_1$, and $\mathbf{RHS}_1$ are calculated for each chain. They are combined as given in Eq. (26).
$\ddot{Y}_1, \lambda$ Eq. (27)		The Base body Cartesian acceleration vector $\ddot{Y}_1$ and Lagrange multiplier vector λ are calculated.
$\ddot{\theta}_{j(j+1)}$ $\ddot{Y}_j$	Eq. (18) Eq. (6)	Using $\ddot{Y}_1$ and λ to start, the relative joint acceleration $\ddot{\theta}_{ij}$ is solved in a forward path sequence down each chain to the chain-end bodies. The Cartesian accelerations must also be calculated since they are required for Eq. (18).
$\dot{q} \rightarrow q$		Relative joint accelerations and velocities are integrated to obtain relative joint velocities and positions. The process is then repeated at a new time step.

3.3 Solution procedure

The solution procedure for the recursive equations of motion is summarized in Table 1.

3.4 Track assembly and dynamic settling simulation

Before the equations of motion for the track are solved, the initial conditions must be known. The assembly of the track around the undercarriage components is first executed to determine its initial configuration prior to the start of each simulation run. The initial configuration of the track must be found in terms of the recursive generalized coordinates. These coordinates must be defined such that the cut-joint constraint equations are satisfied and the track is in the approximate configuration shown in Fig. 2. Several requirements must be met to properly define the coordinates of the track around the undercarriage components. The requirements are that the track pin bushings be placed precisely around the sprocket teeth, the track links must wrap around the idler, and the track must be placed above the carrier roller and below the rollers at the bottom of the undercarriage. The goal of the assembly is to place the links within a prescribed tolerance of the undercarriage components, but not actually touching any part of the undercarriage. If the links are in contact with the undercarriage at the beginning of the simulation, the calculated contact force may be unreasonably large and the program will not behave realistically. When this iterative process is completed, a

dynamic settling simulation is then performed. This produces the shape of the track before starting the full simulation run. The process involves placing the undercarriage just above ground level and simulating the response of the undercarriage as it settles on the ground under the influence of gravity with the sprocket locked against rotation.

3.5 Contact force model

As the sprocket drives the track, the motion of the vehicle is determined by the contact forces between the undercarriage components, track links, and ground. The contact model calculates the force between two rigid bodies from a relative boundary distance δ and velocity $\dot{\delta}_n$ using a stiffness parameter k and damping coefficient c as

$$f_n = k\delta + c\dot{\delta}_n \tag{28}$$

Several contact models were developed to capture the various contacts between the track and the undercarriage as shown in Fig. 6. The following are included: point-segment contact, straight-line segment contact, convex-segment contact, concave-segment contact and sprocket-track contact. Full details of the formulation are given in Sander (1998).

A frictional force between bodies is also calculated using a coefficient of friction and the contact force as the normal force. To avoid numerical difficulties when the direction of the friction force
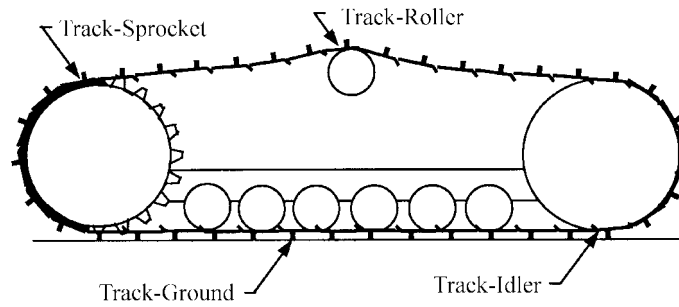

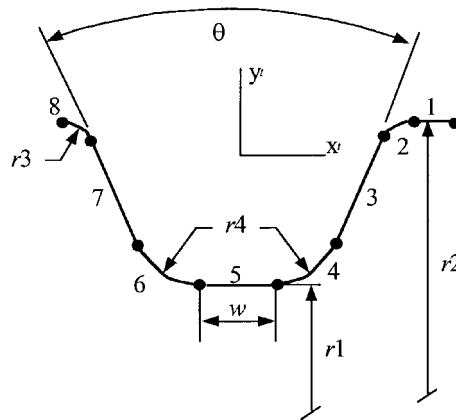Fig. 6 Undercarriage contact types

Fig. 7 Parametrized sprocket tooth geometry

changes, the coefficient of friction is transitioned to zero by use of a hyperbolic tangent function as the tangential relative boundary velocity $\dot{\delta}_t$ approaches zero. In some situations, the contact force is applied at a joint location. When this happens, the force is split evenly and applied to the two bodies connected by the joint. All contact forces are applied at joint locations during track-sprocket interaction in the undercarriage model. This interaction between the sprocket and the track is the most difficult to capture because of the complex geometry involved. The sprocket geometry subroutine allows the following parameters to be defined by the user: number of teeth n_t, tooth face angle θ, radius to the bottom of the tooth r_1, radius to the top of the tooth r_2, radius of a round at the top of the tooth r_3, radius of the seating curve r_4, and the width of a flat section between the teeth w. These parameters are shown for one sprocket tooth valley in Fig. 7.

When a valid set of tooth parameters is entered, the program generates all the points necessary to define the segments that make up complete sprocket geometry. The parameterized sprocket tooth profile developed here consists of 8 controls points and hence, is more realistic than the 3 flat surfaces used in the study by Nakanishi and Shabana (1994b). The sprocket profile can be easily changed for various studies using this method of geometry definition.

The track links are modeled as segment bodies for contact with the rollers and the idler, and the track joint bushings are the point bodies for contact with the sprocket. The geometry of a track link is shown in Fig. 8. Three segments are defined at the top of the link that are used for determining contact with the rollers and idler. A point is defined corresponding to the grouser tip, which is used for calculating the ground contact forces. The joint locations both have point-circle radii associated with them. These point-circles are only used for determining contact with the sprocket. The rollers and idler of the undercarriage are modeled as point-circles. These point-circles are fixed to the undercarriage such that they do not rotate. For this reason, when contact between the track links and the rollers or idler is discussed, the term undercarriage geometry is used to refer to the rollers and idler.

Finally, prior to computing δ between a point-circle and a segment, several checks are incorporated into the model to verify that contact exists. These checks are incorporated to reduce the number of computations when contact is not present. They verify conditions that are necessary for contact, but are not sufficient for making a conclusion on the existence of contact between bodies. Once the relative boundary distance is calculated, contact exists if the distance is between zero and a maximum depth of penetration δ_{max}. The relative boundary distance, velocity, and the
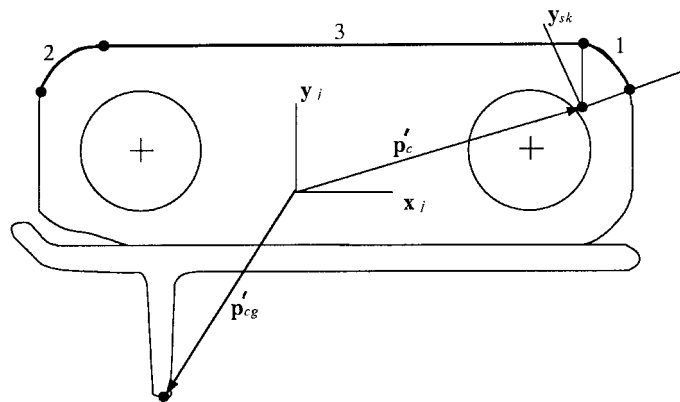

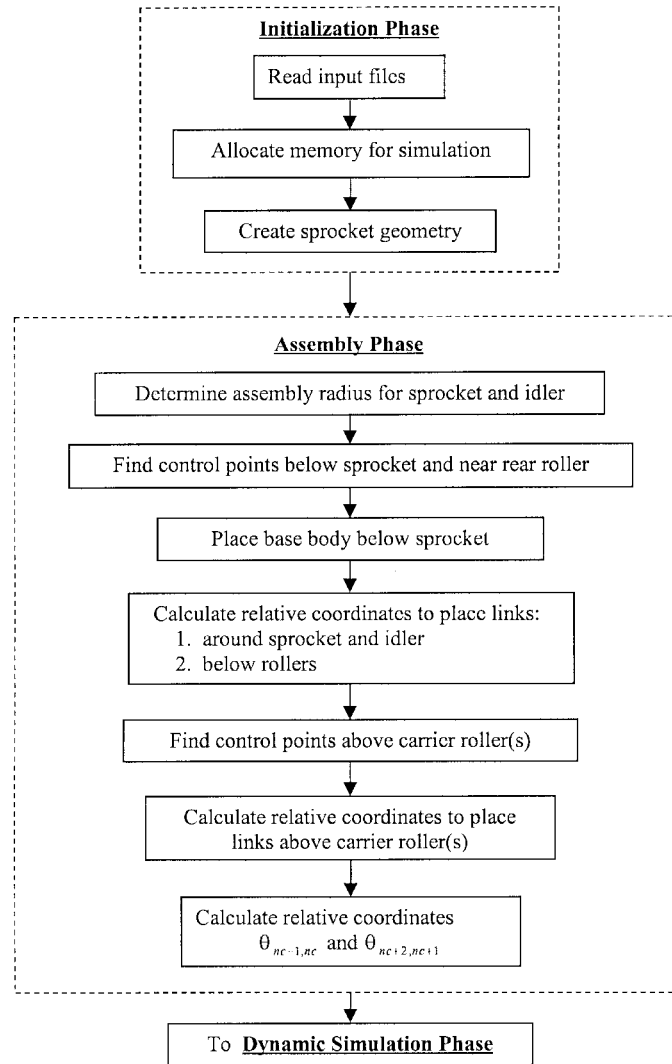Fig. 8 Track link/shoe geometry

Fig. 9 Initialization and assembly phases

associated contact force are only calculated once contact is proven to exist by these checks. The maximum penetration depth is defined to prevent the point-circle from making an initial contact with the material side of a segment.

3.6 Computer implementation

The Adam's-Bashforth-Moulton predictor corrector algorithm is employed to compute the position and velocity. All results presented here are ran using a relative integration tolerance of 1.0×10^{-9} to control the local error at each time step. The overall structure of the program is shown in the flowcharts of Figs. 9 and 10. The order of calculations used for the assembly and dynamic simulation phases is described in these figures. Fig. 9 shows the first two phases of an undercarriage simulation and Fig. 10 depicts the dynamic simulation phase. Within each phase, the major tasks of
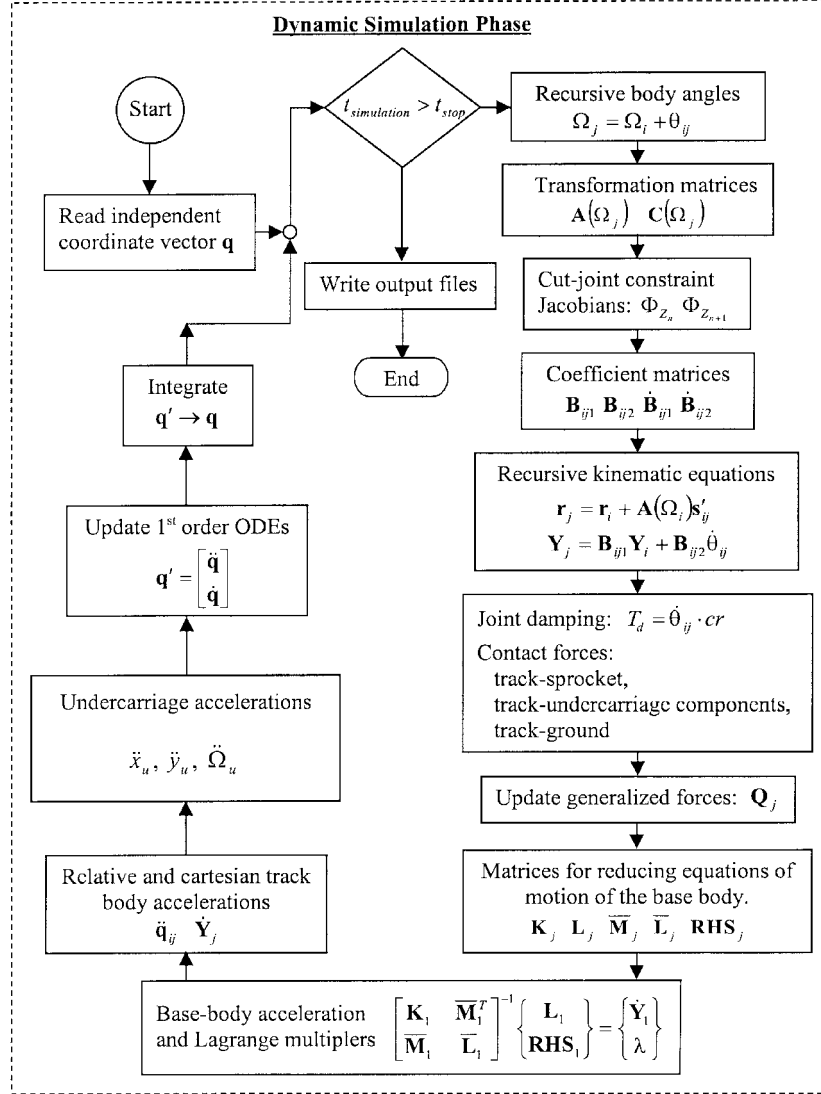
Fig. 10 Dynamic simulation phase

the program are listed to present the overall structure of the program.

4. Modeling the vehicle subsystem

The vehicle subsystem comprises the following parts: cab, chassis, sprocket, idler, undercarriage frame, lower rollers and carrier roller. As depicted in Fig. 11, the cab and the chassis are rigidly connected together, and they are in turn, joined to the undercarriage frame by a revolute joint and a spring-damper unit. This construction permits the vehicle subsystem to be further divided into 2 parts; S_1 which contains the idler, undercarriage frame and lower rollers, and S_2 which consists of
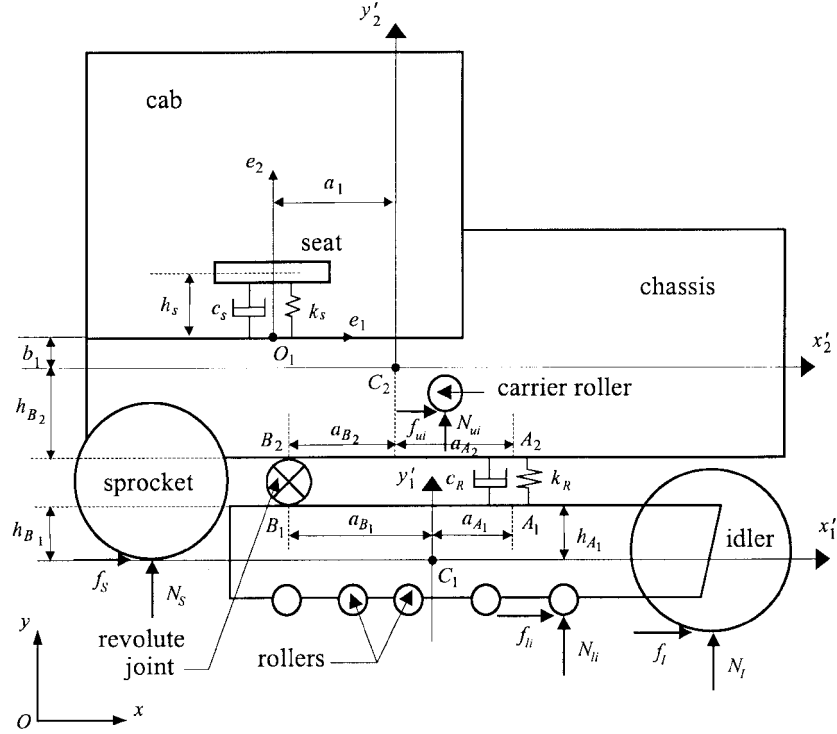
Fig. 11 Model of the vehicle subsystem

the cab, chassis, sprocket and carrier roller. Let the velocity of mass center C_1 and pitch angle of S_1 be $\{u_1, v_1\}$ and θ_1 respectively. Likewise, for S_2 the corresponding quantities for C_2 and pitch angle are $\{u_2, v_2\}$ and θ_2. The equations of motion for the vehicle subsystem are (Han and Mao 1998):

$$u_2 = a_{B_2}\cos\theta_2 - h_{B_2}\sin\theta_2 - a_{B_1}\cos\theta_1 - h_{B_1}\sin\theta_1 + u_1 \tag{29}$$

$$v_2 = a_{B_2}\sin\theta_2 + h_{B_2}\cos\theta_2 - a_{B_1}\sin\theta_1 + h_{B_1}\cos\theta_1 + v_1 \tag{30}$$

$$(m_{S_1} + m_{S_2})\ddot{u}_1 + m_{S_2}(a_{B_1}\sin\theta_1 - h_{B_1}\cos\theta_1)\ddot{\theta}_1 - m_{S_2}(a_{B_2}\sin\theta_2 + h_{B_2}\cos\theta_2)\ddot{\theta}_2$$
$$= f_{C_1 x} + f_{C_2 x} - m_{S_2}(a_{B_1}\dot{\theta}_1^2\cos\theta_1 + h_{B_1}\dot{\theta}_1^2\sin\theta_1 - a_{B_2}\dot{\theta}_2^2\cos\theta_2 + h_{B_2}\dot{\theta}_2^2\cos\theta_2), \tag{31}$$

$$(m_{S_1} + m_{S_2})\ddot{v}_1 - m_{S_2}(a_{B_1}\cos\theta_1 + h_{B_1}\sin\theta_1)\ddot{\theta}_1 + m_{S_2}(a_{B_2}\cos\theta_2 - h_{B_2}\sin\theta_2)\ddot{\theta}_2$$
$$= f_{C_1 y} + f_{C_2 y} - m_{S_1}(a_{B_1}\dot{\theta}_1^2\sin\theta_1 - h_{B_1}\dot{\theta}_1^2\cos\theta_1 - a_{B_2}\dot{\theta}_2^2\sin\theta_2 - h_{B_2}\dot{\theta}_2^2\cos\theta_2), \tag{32}$$

$$m_{S_2}h_{B_1}\ddot{u}_1 + m_{S_2}a_{B_1}\ddot{v}_1 - \left\{ m_{S_2}\left[(a_{B_1}\cos\theta_1 + h_{B_1}\sin\theta_1)a_{B_1} - (a_{B_1}\sin\theta_1 - h_{B_1}\cos\theta_1)h_{B_1}\right] + I_{z1} \right\}\ddot{\theta}_1$$
$$+ m_{S_2}\left[(a_{B_2}\cos\theta_2 - h_{B_2}\sin\theta_2)a_{B_1} - (a_{B_2}\sin\theta_2 + h_{B_2}\cos\theta_2)h_{B_1}\right]\ddot{\theta}_2$$
$$= -M_{C_1 z} + f_{C_2 x}h_{B_1} + f_{C_2 y}a_{B_1} + f_{A_{12} x}(h_{A_1} + h_{B_1}) + f_{A_{12} y}(a_{A_1} + a_{B_1}) \tag{33}$$

$$-m_{S_2}\left(a_{B_1}\dot{\theta}_1^2\sin\theta_1-h_{B_1}\dot{\theta}_1^2\cos\theta_1-a_{B_2}\dot{\theta}_2^2\sin\theta_2-h_{B_2}\dot{\theta}_2^2\cos\theta_2\right)a_{B_1}$$

$$-m_{S_2}\left(a_{B_1}\dot{\theta}_1^2\cos\theta_1+h_{B_1}\dot{\theta}_1^2\sin\theta_1-a_{B_2}\dot{\theta}_2^2\cos\theta_2+h_{B_2}\dot{\theta}_2^2\sin\theta_2\right)h_{B_1},$$

$$m_{S_2}h_{B_2}\ddot{u}_1-m_{S_2}a_{B_2}\ddot{v}_1+m_{S_2}\left[\left(a_{B_1}\cos\theta_1+h_{B_1}\sin\theta_1\right)a_{B_2}+\left(a_{B_1}\sin\theta_1-h_{B_1}\cos\theta_1\right)h_{B_2}\right]\ddot{\theta}_1$$

$$-\left\{m_{S_2}\left[\left(a_{B_2}\cos\theta_2-h_{B_2}\sin\theta_2\right)a_{B_2}+\left(a_{B_2}\sin\theta_2+h_{B_2}\cos\theta_2\right)h_{B_2}\right]+I_{z2}\right\}\ddot{\theta}_2$$

$$=-M_{C_2z}+f_{C_2x}h_{B_2}-f_{C_2y}a_{B_2}-f_{A_{12}x}\left(h_{A_2}-h_{B_2}\right)-f_{A_{12}y}\left(a_{A_2}+a_{B_2}\right)$$

$$+m_{S_2}\left(a_{B_1}\dot{\theta}_1^2\sin\theta_1-h_{B_1}\dot{\theta}_1^2\cos\theta_1-a_{B_2}\dot{\theta}_2^2\sin\theta_2-h_{B_2}\dot{\theta}_2^2\cos\theta_2\right)a_{B_2}$$

$$-m_{S_2}\left(a_{B_1}\dot{\theta}_1^2\cos\theta_1+h_{B_1}\dot{\theta}_1^2\sin\theta_1-a_{B_2}\dot{\theta}_2^2\cos\theta_2+h_{B_2}\dot{\theta}_2^2\sin\theta_2\right)h_{B_2}, \quad (34)$$

where

$$m_{S_1}=m_{\text{idler}}+m_{\text{undercarriage}}+\sum_{i=1}^{n_l}m_{\text{lowroll}_i}, \quad m_{S_2}=m_{\text{cab}}+m_{\text{chassis}}+m_{\text{sprocket}}+\sum_{i=1}^{n_u}m_{\text{uproll}_i},$$

$$f_{C_1x}=f_I+\sum_{i=1}^{n_l}f_{li}, \quad F_{C_1y}=N_I+\sum_{i=1}^{n_l}N_{li}, \quad f_{C_2x}=f_S+\sum_{i=1}^{n_u}f_{ui}, \quad F_{C_1y}=N_s+\sum_{i=1}^{n_u}N_{ui},$$

$$M_{C_1z}=-f_I\left(y_I-y_{C_1}\right)-\sum_{i=1}^{n_l}f_{li}\left(y_{li}-y_{C_1}\right)+N_I\left(x_I-x_{C_1}\right)+\sum_{i=1}^{n_l}N_{li}\left(x_{li}-x_{C_1}\right),$$

$$M_{C_2z}=-f_S\left(y_S-y_{C_2}\right)+-\sum_{i=1}^{n_u}f_{ui}\left(y_{ui}-y_{C_2}\right)+N_S\left(x_S-x_{C_2}\right)+\sum_{i=1}^{n_u}N_{ui}\left(x_{ui}-x_{C_2}\right).$$

The spring-damper force on subsystems S_1 and S_2 is

$$f_{A_1A_2}=k_R\left(r_{A_1A_2}-r_{A_1A_20}\right)+c_R\dot{r}_{A_1A_2}. \quad (35)$$

Also, the equation of motion for the seat of mass m_s is given by

$$m_S\ddot{u}_{S2}+c_S\dot{u}_{S2}+\left(k_S-m_S\dot{\theta}_2^2\right)u_{S2}=m\left(h_S\dot{\theta}_2^2+\ddot{u}_2\sin\theta_2-\ddot{v}_2\cos\theta_2+\ddot{\theta}_2a_1+\dot{\theta}_2^2b_1\right), \quad (36)$$

in which u_{S2} is the displacement of seat in the direction of e_2 relative to the cab.

5. Modeling the tracked vehicle-ground interaction

A further improvement of the track-ground model can be obtained by computing the contact force via a Winkler-type foundation with springs and dampers (not shown). As illustrated in Fig. 12, the
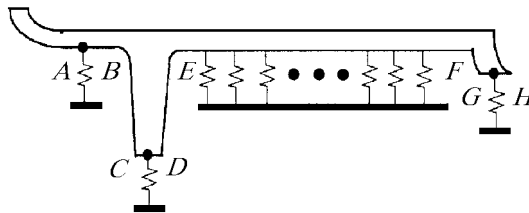

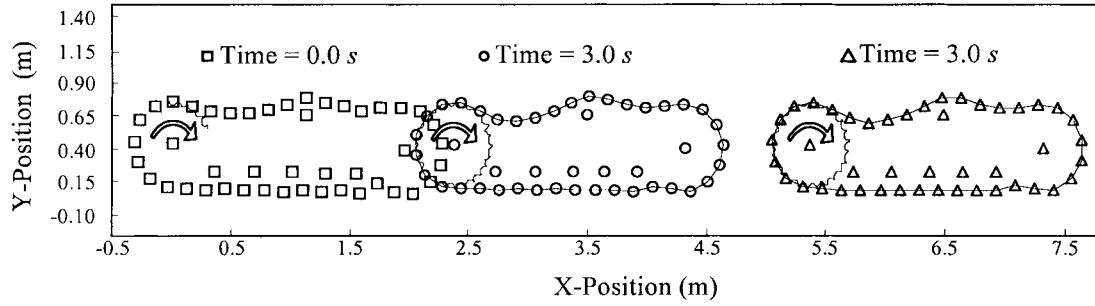Fig. 12 Track-ground interaction model

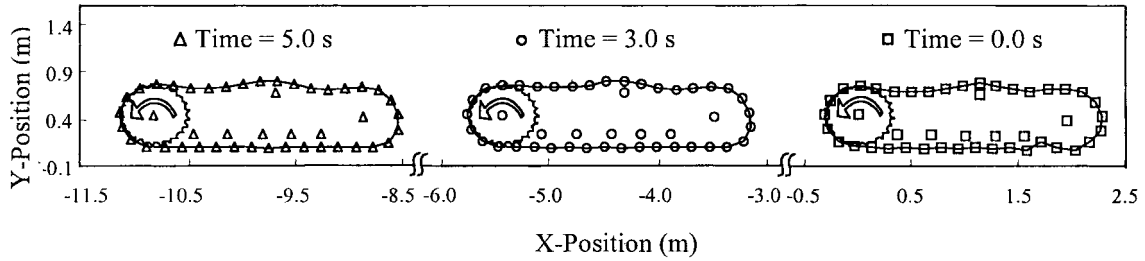Fig. 13 Undercarriage motion forward direction

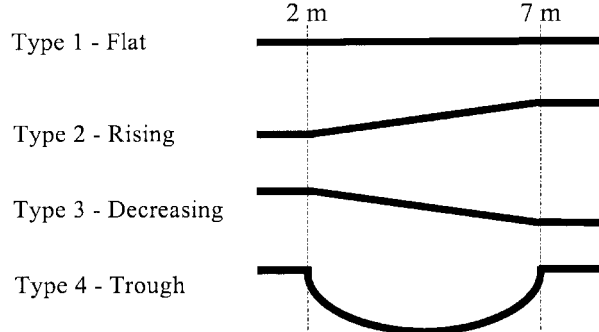Fig. 14 Undercarriage motion in reverse direction

Table 2. Road profiles used

contacts in segments *AB*, *CD* and *GH* with ground are modeled by concentrated contact forces and in segment *EF* by distributed contact forces.

6. Simulation runs of the track subsystem

Figs. 13 and 14 depict simulation runs of the track subsystem in forward and reverse motions respectively, on a flat ground. The sprocket starts from rest and increases linearly until it attains a final operating velocity of 3.14 rad/s in 0.75 s.
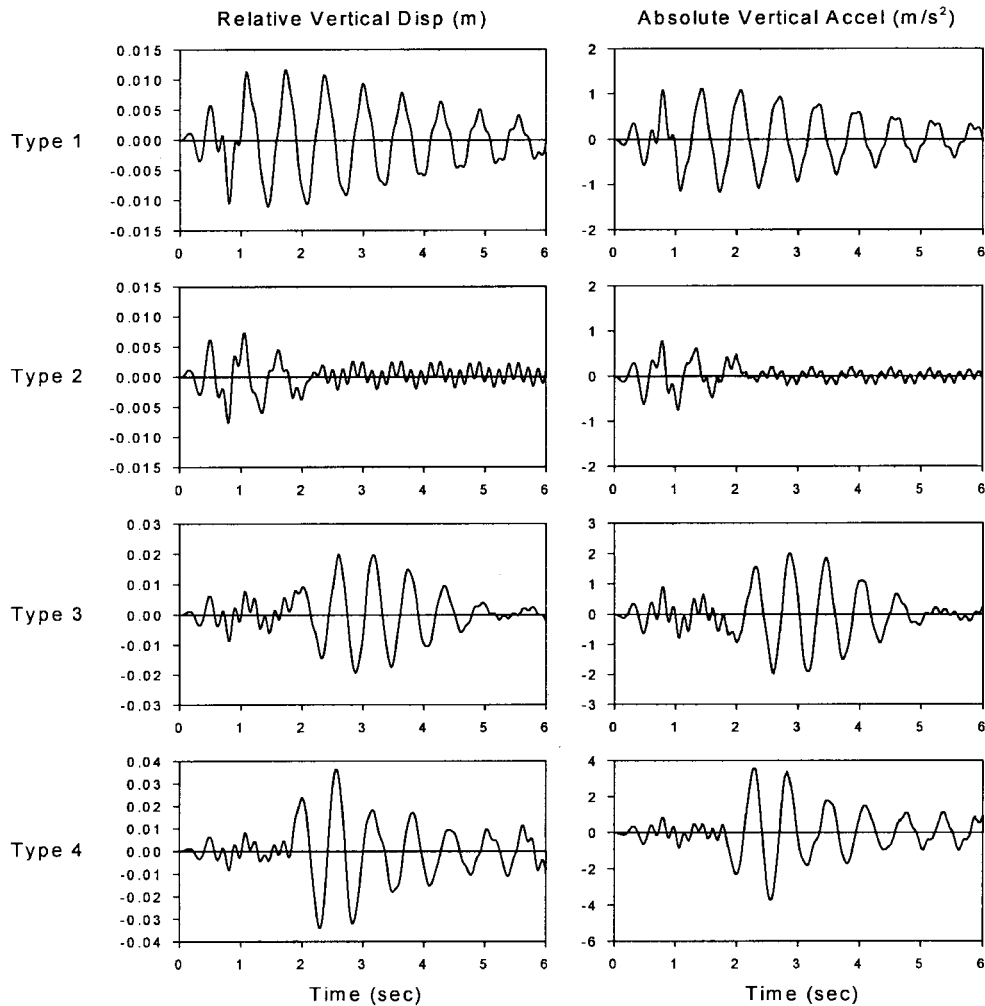
Fig. 15 Seat vibrations for a crawler traversing varying road profiles

7. Simulation runs of the integrated tracked vehicle system

Simulation runs of the integrated tracked vehicle system for vibration characteristics for varying flexible road profiles are investigated here. However, due to page limitation, only the results of the seat vibrations are provided. As listed in Table 2, four types of road profiles are used in the study. The results for the relative vertical displacements and the absolute vertical accelerations are plotted in Fig. 15. FFT results have also been generated but are not presented here. Of the 4 road profiles studied, it is not surprising to observe that tracked vehicles traversing a trough produce the greatest seat vibrations.

8. Conclusions

The objectives of this work are twofold: to develop a high-fidelity multibody model of a tracked vehicle and to study its interaction with a flexible ground terrain with a varying profile. Since the investigation is restricted to off-road vehicles that are slow-moving, it is crucial that the each link of the track subsystem be individually modeled. This can lead to increased computational difficulties. To minimize them and thus, enhance the overall efficiency and viability of the modeling, a recursive formulation is employed for the track subsystem. Simulation runs of the track subsystem in forward and reverse motions are presented. Additionally, simulation runs of the integrated tracked vehicle system for four flexible ground profiles are generated. Results of the seat vibration for each of the varying terrain conform well to the general expectations.

References

Bae, D.S. and Haug, E.J. (1987), "A recursive formulation for constrained mechanical system dynamics. Part II: closed loop systems", *Mechanics of Structures and Machines*, **15**.

Creighton, D.C. (1986), "Revised vehicle dynamic module: User's guide for computer program VEHDYN II", WES Technical Report No. SL-86-9, U.S. Army Engineer Waterways Experiment Station, Vicksburg, MS.

Dhir, A. and Sankar, S. (1994), "Analytical track models for ride dynamic simulation of tracked vehicles", *Journal of Terramechanics*, **31**.

Galaitsis, A.G. (1984), "TRAXION: A model for predicting dynamic track loads in military vehicles", ASME *Trans, Journal of Vibration, Acoustics, Stress Reliability in Design*, **106**.

Han, Ray P.S. and Zhao, Z.C. (1990), "Dynamics of general flexible multibody systems", *International Journal for Numerical Methods in Engineering*, **30**, 77-97.

Han, Ray P.S. and Mao, S.G. (1998), "Development of an integrated cab-chassis-undercarriage model for a flexible ground terrain", Report #3, John Deere Dubuque Works, Dubuque, IA.

Han, Ray P.S. and Mao, S.G. (1999), "Hamilton equation-based symplectic finite element modeling of flexible multibodies undergoing large overall motion", *IMechE, Journal of Multibody Dynamics*, June (submitted).

Han, Ray P.S., S.G. Mao and Brian S. Sander (1999), "Multibody dynamic modeling of a tracked vehicle traversing a flexible ground terrain with a varying profile", *Proceedings of DAS 1999 at the Fourth Asia-Pacific Conference on Computational Mechanics*, Singapore, December 13-17.

McCullough, M.K., and Haug, E.J. (1985), "Dynamics of high mobility track vehicles", ASME Paper No. 85-DET-95.

Murphy, N.R. and Ahlvin, R.B. (1976), "Vehicle dynamics module", Technical Report No. M-76-1, US Army Engineer Waterways Experiment Station, Vicksburg, MS.

Nakanishi, T. and Shabana, A. (1994a), "Contact forces in the non-linear dynamic analysis of tracked vehicles", *International Journal for Numerical Methods in Engineering*, **37**.

Nakanishi, T. and Shabana, A. (1994b), "On the numerical solution of tracked vehicle dynamic equations", *Nonlinear Dynamics*, **6**.

Sander, B.S. (1998), "A recursive model for the dynamic simulation of a tracked vehicle undercarriage", M.S. Thesis, The University of Iowa, Iowa City, IA.